Jin, M. and Chen, Q. 2014."Accelerating fast fluid dynamics with a coarse-grid projection scheme," *HVAC&R Research*, 20(8), 932-943.

Accelerating Fast Fluid Dynamics with a Coarse-grid Projection Scheme

Mingang Jin, Qingyan Chen*
School of Mechanical Engineering, Purdue University, West Lafayette, IN 47907, USA
*Tel. (765) 496-7562, Fax (765) 494-0539, Email: yanchen@purdue.edu

Abstract

Fast fluid dynamics (FFD) is an intermediate model that can provide fast and informative building airflow simulations. Although reasonably good simulation accuracy is important for FFD, computational efficiency is the primary concern, and it is necessary to further increase FFD speed. Because the most time-consuming part of FFD is solving the stiff pressure equation, this study proposed the application of a coarse-grid projection (CGP) scheme, which solves the momentum equation on the fine grid level and the pressure equation on the coarse grid level. Therefore, appropriate approaches for mapping velocity and pressure information between different grid levels were investigated in this study. To evaluate the accuracy and computational efficiency of FFD with the CGP scheme in simulating building airflows, this study tested it with building airflows of varying complexity. The results showed that the CGP scheme would not have a negative impact on the accuracy of FFD in the simulation of building airflows, and it could significantly reduce the fluctuations that occur within the simulations. The CGP scheme was able to accelerate FFD by approximately 1.5 times, and thus FFD with the CGP scheme achieved a computing speed that was 30 to 50 times faster than computational fluid dynamics (CFD) models.

Introduction

Fast and informative building airflow simulations are required in various applications, such as emergency management, fast design of sustainable buildings, and development of integrated building energy and airflow simulation tools. Fast fluid dynamics (FFD), as an intermediate model between multi-zone models (Axley, 2007) and computational fluid dynamics (CFD) models, is a potential tool for providing fast and informative building airflow simulations.

Initially designed for visualizing fluid flow in real time for computer games (Fedkiw et al., 2001; Stam, 1999), FFD has also been used to perform real-time and faster-than-real-time building airflow simulations (Zuo and Chen, 2009). Rather than producing plausible visual effects, for engineering purposes FFD should achieve reasonable accuracy in simulating the primary characteristics of airflows and predicting airflow parameters such as temperature and velocity. Zuo et al. (2010) implemented a finite volume method and mass correction at the outflow boundary to improve the simulation accuracy of FFD. A hybrid scheme that combined linear and third-order interpolations was also proposed to reduce the numerical diffusion in FFD and provide more accurate simulations for laminar flows with the same special and temporal resolutions (Zuo et al., 2012). To validate the performance of FFD in simulating complex three-dimensional airflows in buildings, Jin et al. (2012a, b) developed FFD into a three-dimensional model and applied it to simulate different types of building airflows. They found that FFD was capable of capturing major airflow features in buildings with a computing speed of over 15 times faster than that of CFD tools. FFD was further validated for simulating airflows in buildings with natural ventilation, and the investigation found that that FFD was capable of predicting the main air flow features and ventilation rate with reasonable accuracy for wind-driven or buoyancy-driven natural ventilation (Jin et al., 2013).

Although reasonable simulation accuracy is important for FFD, computational efficiency is the primary concern. In one approach to improving the computing speed of FFD, Zuo et al. (2010) modified the time-splitting scheme. In a second approach, FFD was implemented in parallel on a graphics processing unit (GPU) to further accelerate FFD simulations. FFD on a GPU could achieve a computing speed of 10-30 times faster than on a central processing unit (CPU) (Zuo and Chen, 2010a, b). Although it might seem more efficient to increase the speed of FFD by parallel computing, enhancement of the algorithm can improve the computational efficiency of FFD on a fundamental level. Therefore, it is necessary to further explore the potential improvements of FFD algorithms. Currently, the most time-consuming part of FFD is solving the diffusion and pressure equations. Although FFD applies the same iterative approach to solve

both the implicit diffusion equations and the pressure equation, the pressure equation is much stiffer to solve than the diffusion equations. Because the convergence of the pressure equation is much slower than that of the diffusion equations, many more iterations of the equation solver are required in order to achieve sufficient precision. Obtaining convergence consumes a major portion of the total computing effort of FFD. Therefore, an efficient approach to solving the pressure equation could significantly reduce the computing time of FFD.

Using an advanced equation solver to solve the pressure equation is a potential approach. Multi-grid methods, which are considered to be the most effective equation solvers, have been investigated by many researchers in an attempt to reduce the computing effort required to solve pressure equations (Behie and Forsyth, 1983; Fuchs and Zhao, 1984; Sidilkover and Ascher, 1995). In addition, MacLachlan et al. (2008) applied a multi-grid preconditioned conjugate gradient method (Tatebe, 1993) to reduce the computing cost in solving a Poisson equation, and they found that it could efficiently calculate two-phase flows on highly resolved grids. McAdams et al. (2010) presented a parallel multi-grid solver and demonstrated its efficiency with animations of smoke flow past solid objects and free surface water. Although multi-grid methods are very efficient, they require the exchange of additional boundary information during the solving process. Exchanging boundary information can result in a computational bottleneck in practical application and leads to an even higher computing cost (Lentine et al., 2010). In contrast, by solving the pressure equation directly on a coarser grid level, the coarse-grid projection (CGP) scheme can significantly reduce the size of the pressure equation and thus accelerate the speed of flow simulations. Lentine et al. (2010) proposed the CGP scheme and applied it to three-dimensional flow simulations for computer games. The simulations require only a fraction of the computing effort of those with a full projection scheme but can still obtain fine-scale flow structures and details. San and Staples (2013a) demonstrated that the CGP scheme could accelerate incompressible flow computations while retaining a level of accuracy close to that of fine grid projection. San and Staples (2013b) also applied the CGP scheme in quasigeostrophic models for simulating large-scale ocean circulation, and they found that the scheme could increase computing speed while achieving the same level of accuracy in the fine-resolution field and effectively eliminating numerical oscillation due to lower grid resolutions. Therefore, the CGP scheme has potential for further increasing the speed of FFD simulations.

Although the CGP scheme has been implemented by other researchers, the current study integrated the scheme with FFD. The momentum equation is solved on the fine grid level in FFD, and the pressure equation is solved on the coarse grid level with the CGP scheme. Therefore, this study investigated appropriate schemes for mapping velocity and pressure information between different grid levels. To evaluate the accuracy and computational efficiency of FFD with the CGP scheme in simulating building airflows, it is necessary to test the model with airflows of varying complexity. This requirement forms the basis of the current investigation, as reported in this paper.

Research Methods

Fast Fluid Dynamics. Fast fluid dynamics simulates airflow movement by numerically solving the incompressible Navier-Stokes (NS) equation (1) and continuity equation (2) given below:

$$\frac{\partial U_i}{\partial t} + U_j \frac{\partial U_i}{\partial x_j} = -\frac{1}{\rho}\frac{\partial p}{\partial x_i} + \nu \frac{\partial^2 U_i}{\partial x_j \partial x_j} + \frac{1}{\rho} F_i , \tag{1}$$

$$\frac{\partial U_i}{\partial x_i} = 0 , \tag{2}$$

where i, j = 1, 2, 3 for three orthogonal directions, x_i or x_j. The variable U_i is the ith component of the velocity vector; p is pressure, ρ density, F_i the ith component of the body forces, and ν the kinetic viscosity, respectively. To enhance computational efficiency in solving the momentum equation (1), a time-splitting scheme (Ferziger and Perić, 1999) is applied to split Eq. (1) into an advection equation (3), diffusion equation (4), and pressure correction equation (5), which are solved sequentially in each time step.

$$\frac{U_i^{(1)} - U_i^n}{\Delta t} = -U_j \frac{\partial U_i^n}{\partial x_j} , \tag{3}$$

$$\frac{U_i^{(2)} - U_i^{(1)}}{\Delta t} = \nu \frac{\partial^2 U_i^{(2)}}{\partial x_j \partial x_j} + F_i, \tag{4}$$

$$\frac{U_i^{n+1} - U_i^{(2)}}{\Delta t} = -\frac{1}{\rho} \frac{\partial p}{\partial x_i}. \tag{5}$$

where U_i^n and U_i^{n+1} represent the velocity at the previous and current time steps, respectively. FFD first solves the convection equation (3) by using a semi-Lagrangian scheme (Staniforth and Côté, 1991) to obtain intermediate velocities $U_i^{(1)}$. Then the intermediate velocities are further updated with $U_i^{(2)}$ by implicitly solving the diffusion equation (4). In the third step, a pressure correction (Chorin, 1967) is performed to obtain U_i^{n+1}. To solve the pressure term in Eq. (5), a pressure projection is applied to enforce the divergence-free velocity field. By taking divergence on both sides of Eq. (5), a Poisson equation (6) can be derived when Eq. (2) is satisfied.

$$\frac{\partial^2 P}{\partial x_j \partial x_j} = \frac{\rho}{\Delta t} \frac{\partial U_j^{(2)}}{\partial x_j}. \tag{6}$$

The Poisson equation requires a large computing effort to solve. By improving the computational efficiency in solving Eq. (6), FFD can significantly increase computing speed. After the velocity field has been obtained, transport equations for the other scalars are solved in a similar manner.

This study applied Boussineque approximation (Gray and Giorgini, 1976) to realize the coupling between the energy equation and the momentum equaions. The bouyancy force generated by temperature differences was added as a source term to the body force term Fi in Eq. (1). During ther simualtion, the buoyance force for each cell would be updated at the beginning of each time step.

Coarse-Grid Projection. Lentine et al. (2010) introduced the scheme of CGP for simulating incompressible flow. By solving the pressure equation on the coarse grid level, the size of the discretized pressure equation can be significantly reduced, which in turn decreases the computing effort. As shown in Figure 1, one level of binary coarsening is applied on the original fine grids in FFD. In two-dimensional meshes, each coarse cell contains four cells at the fine grid level, and the surfaces of the coarse cell overlap with the outer faces of the fine cells. Similarly, eight fine cells form one coarse cell in three-dimensional meshes. In FFD, the velocity components and pressure are stored on both coarse and fine grid levels, with velocity components at the cell faces and pressure at the cell center. FFD with the coarse-grid projection scheme solves only the momentum equations on the fine grids, while solving the pressure equation on the coarse grids. As in the multi-grid method, restriction and prolongation are required to transfer information about velocity and pressure between the fine and coarse grids.

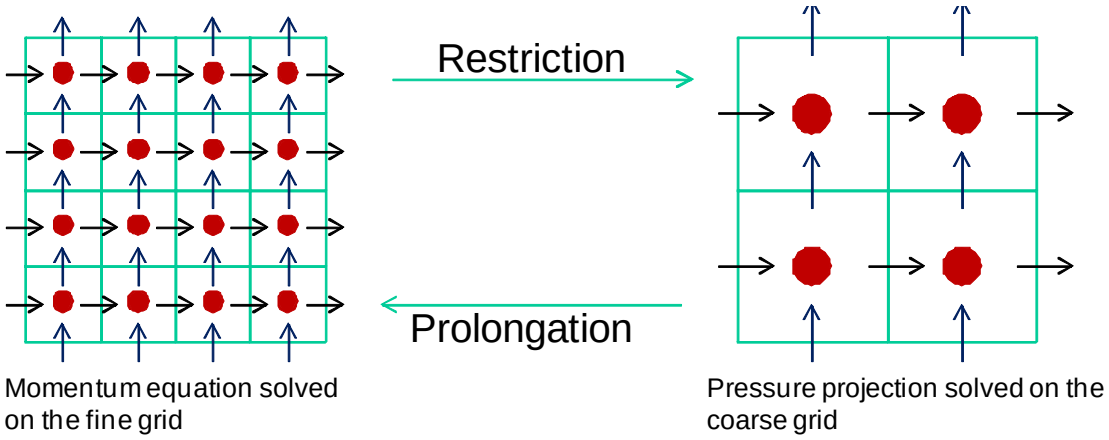

Figure 1. Illustration of the CGP scheme.

After solving the momentum equations and obtaining the intermediate velocities, FFD applies four steps in order to perform CGP and achieve a divergence-free velocity field: restriction, pressure projection, prolongation, and local projection. Since the pressure projection is conducted on the coarse grid level, the intermediate velocities $u_{fi}^{(2)}$ on the fine grid level should be restricted to the coarse grid. In FFD, the velocity at the coarse cell face is represented by the area-weighted average of velocities at the fine cell faces overlapping with the coarse grid cell face, which is given by:

$$U_{ic} = \frac{1}{A_c} \sum A_f U_{if}^{(2)}, \tag{7}$$

where U_{ic} and U_{if} are the velocities at the coarse cell surface and fine cell surfaces respectively. The variables A_c and A_f are the areas of the coarse cell surface and fine cell surfaces, respectively, where A_c equals the summation of A_f of all fine cell faces overlapping with the coarse cell face. The restriction that results from using the area-weighted average ensures that the mass flow rate through the face of the coarse cell is equal to that of the overlapping fine cell faces. After mapping the velocity from fine grids to coarse grids, the pressure projection is applied by solving Eq. (8),

$$\frac{\partial^2 P_c}{\partial x_j \partial x_j} = \frac{\rho}{\Delta t} \frac{\partial U_{cj}}{\partial x_j}, \tag{8}$$

where P_c is the pressure stored on the coarse grid level. With fewer cells at the coarse grid level, Eq. (8) can be solved much more efficiently than Eq. (6). The solved pressure distribution on the coarse grid level is then applied to determine the corrections for the coarse grid velocities in order to satisfy the conservation of mass on the coarse grid level. The same correction is prolongated to the fine grid level and applied to the velocities at the fine cell faces that overlap the coarse cell faces, as expressed by Eq. (9),

$$U_{if}^{n+1} = U_{if}^{(2)} - \frac{\Delta t}{\rho} \frac{\partial P_c}{\partial x_i}. \tag{9}$$

Therefore the velocities at the perimeter faces of the fine cells contained in each coarse cell can be updated to the current time step. Because the correction does not cause the mass flow rate to change during the prolongation, the velocities at the perimeter faces satisfy the conservation of mass. However, the velocities at the inner fine faces within the coarse cell have not been updated and might not be divergence free. As shown in Figure 2, one coarse cell contains four fine cells. After the prolongation, the eight perimeter velocities have been determined, but the inner velocities, including u_1, u_2 , u_3, and u_4, have not been corrected to satisfy mass conservation at the fine grid level.

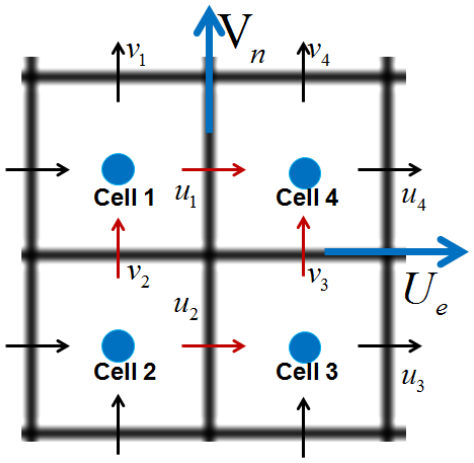

Figure 2. Illustration of the local projection scheme.

In order to obtain a divergence-free field on the fine grid level, a local projection is applied to correct the inner velocities within each coarse cell. For each coarse cell, as shown in Figure 2, it is considered that there is a unique computational domain. Since the perimeter velocities have been determined, they can be considered as fixed velocity boundary conditions for this domain. By applying Eq. (6) for the fine cells within each coarse cell, the pressure distribution on the fine grids can be calculated. On the basis of Eq. (5), the inner velocity can be further corrected to achieve mass conservation on the fine grid level. Since the discretized pressure equation for the local projection has only eight unknowns on the three-dimensional meshes, it can be solved quickly. Therefore, after the four steps of CGP have been performed, the velocities at the fine grids can be corrected efficiently to achieve a divergence-free velocity field in the entire computational domain.

Results

Although the CGP scheme is a promising method for reducing the computing time of FFD, it might degrade the simulation accuracy because the pressure equation is solved on the coarse grid level. Thus, it is necessary to evaluate the impact of the scheme on the accuracy of FFD in simulating building airflows. This study applied FFD with the CGP scheme to simulate the following airflows: a lid-driven cavity flow that represents a typical room airflow pattern from a wall jet; forced and mixed ventilation in a chamber; wind-driven cross ventilation in a wind tunnel; and buoyancy-driven, single-sided ventilation in a full-scale chamber.

Lid-Driven Cavity Flow. This study first investigated the accuracy of FFD with the CGP scheme by simulating a lid-driven cavity flow, which is one of the classical benchmark cases for numerical solvers of Navier-Stokes equations. Ku et al. (1987) numerically investigated three-dimensional lid-driven cavity flow with a Chebyshev pseudo-spectral technique and obtained a high-quality velocity distribution in the cavity with Reynolds numbers from 100 to 1000. As shown in Figure 3, this study adopted the same cubic cavity as Ku et al. (1987) for testing the performance of FFD with the CGP scheme. The dimensions of the cavity were 1 m × 1 m × 1 m, and the Reynolds number based on the cavity size and the moving speed of the top lid was 1000. A fine grid of 32 × 32 × 32 was used in the simulation, and a corresponding coarse grid of 16 × 16 × 16 was automatically generated.

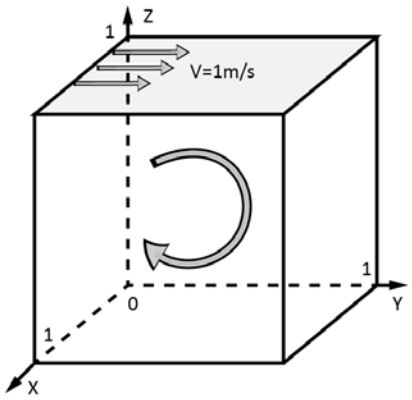

Figure 3. Schematic of the flow in a cubic lid-driven cavity.

Figure 4 compares velocity profiles simulated by FFD with and without the CGP scheme, with the high-accuracy simulation data from Ku et al. (1987). Figure 4(a) depicts the velocity distribution at the vertical center line. FFD with the CGP scheme predicted the same velocity profile as did the original FFD model. Both models obtained good agreement with the reference data, except for some discrepancies at the bottom of the cavity, where they both predicted a lower velocity. For the velocity distribution at the horizontal center line, as shown in Figure 4(b), both models also predicted a very similar profile. Because of the existence of numerical diffusivity in FFD, neither model could accurately simulate the high velocity gradient region in the cavity, and both models under-predicted the peak velocity near the right and left walls as compared with the reference data. Overall, the CGP scheme did not cause a negative impact on the accuracy of FFD for simulating flows in a lid-driven cavity.

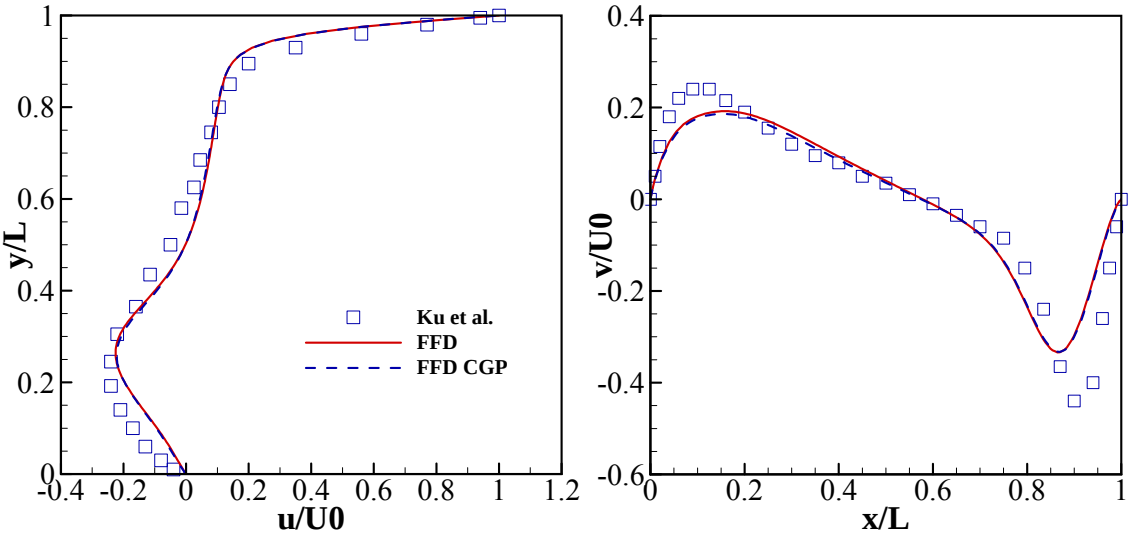

(a) (b)

Figure 4. Velocity variation at (a) the vertical centerline and (b) the horizontal centerline in a lid-driven cavity: comparison of FFD predictions with data from Ku et al. (1987)

Forced and Mixed Ventilation in a Chamber. Airflows in a ventilated room are usually driven by multiple forces, and the interaction of these driving forces can generate complex airflow features. Thus it was necessary for this study to further test FFD with the CGP scheme by simulating realistic airflows in a ventilated room. Wang and Chen (2009) designed and conducted experiments to investigate the airflows in a chamber with added features, as follows: (a) forced ventilation in an empty room; (b) forced ventilation in a room with a box; and (c) mixed ventilation in a room with a heated box. As shown in Figure 5(a), air was supplied to a chamber with dimensions of 2.44 m × 2.44 m × 2.44 m from an inlet at a height of 0.03 m in the upper left corner and the jet flow developed along the ceiling, reaching the far right side of the chamber. The exhaust was located at a height of 0.08 m in the lower right corner of the chamber. Initially the room was empty, and a circulation pattern was formed inside. The inlet air velocity was 0.455 m/s with a corresponding Reynolds number of approximately 2,000. A grid size of 26 × 34 × 26 was used for simulation.

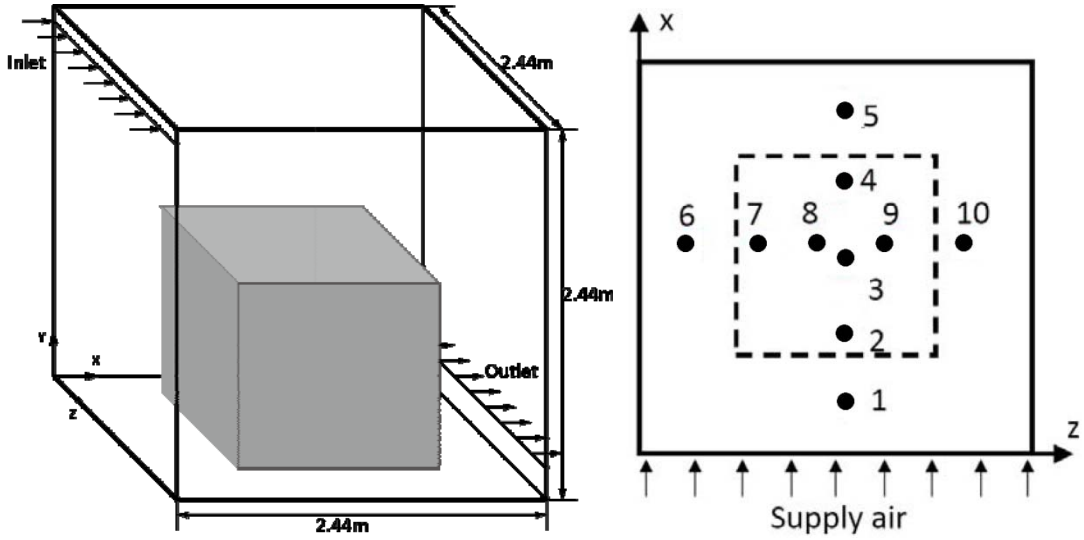

(a) (b)

Figure 5. Schematic of the test chamber and the measurement positions.

FFD with and without the CGP scheme was applied to simulate the airflows in this empty room with forced ventilation, and the predicted velocity profiles at three measurement positions were compared with the experimental data, as presented in Figure 6. These positions are identified as 1, 3, and 5 and are located at the jet upstream, jet downstream, and room center, respectively, as illustrated in Figure 5(b). In this case, FFD with CGP predicted velocity profiles that were similar to those predicted by the original FFD model. Both models captured the high speed of the jet from the inlet, and the simulated profiles agreed well with the experimental data at Positions 1 and 3. However, at Position 5, where flow separation and reattachment occurred, neither model obtained good agreement with the experiment data. Without the integration of sophisticated turbulence models, it was not possible for FFD to predict such complex flow structures accurately.

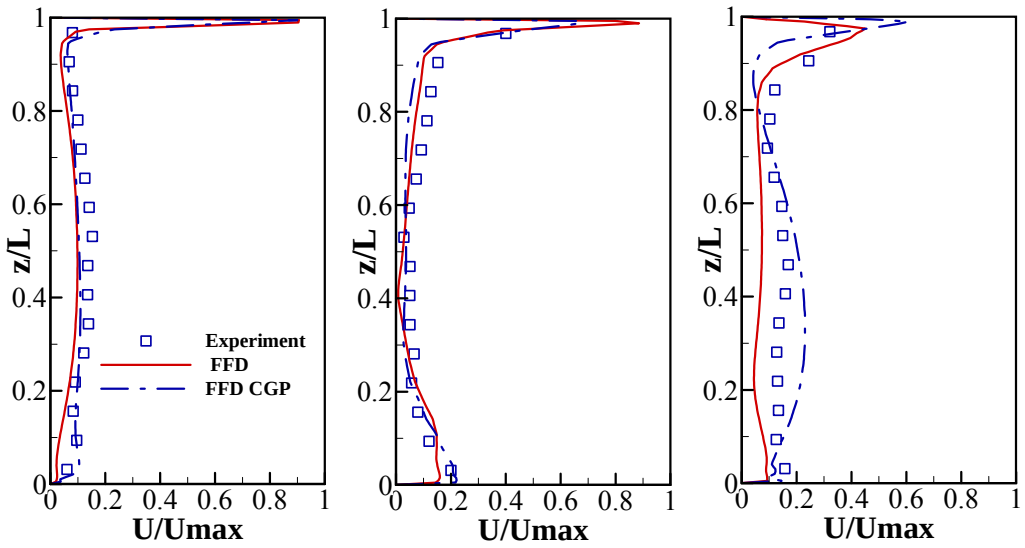

Figure 6. Velocity profiles in the empty room under forced convection: comparison of predictions by the FFD models with the experimental data from Wang and Chen (2009) at Positions (a) 1, (b) 3, and (c) 5.

To increase airflow complexity, a box was added in the center of the chamber to represent obstacles such as furniture and occupants, as illustrated in Figure 5(a). Similarly, FFD with the CGP scheme was applied to simulate this case with a grid size of 28 × 36 × 28, and the simulated velocity profiles were compared with the profile predicted by the original FFD and with the experimental data, as shown in Figure 7. FFD with CGP was able to predict the high air velocity in the jet region but tended to under-estimate the velocity at Positions 1 and 5 as compared with the experimental data. FFD with a standard pressure projection also under-predicted the velocities at these two locations. This under-prediction occurred because the low-order algorithm in FFD generated considerable numerical diffusivity, which caused the air velocity near the wall to be significantly dampened. A comparison of the profiles predicted by the two FFD models shows that the CGP scheme would not cause significant degradation in the accuracy of FFD in this case.

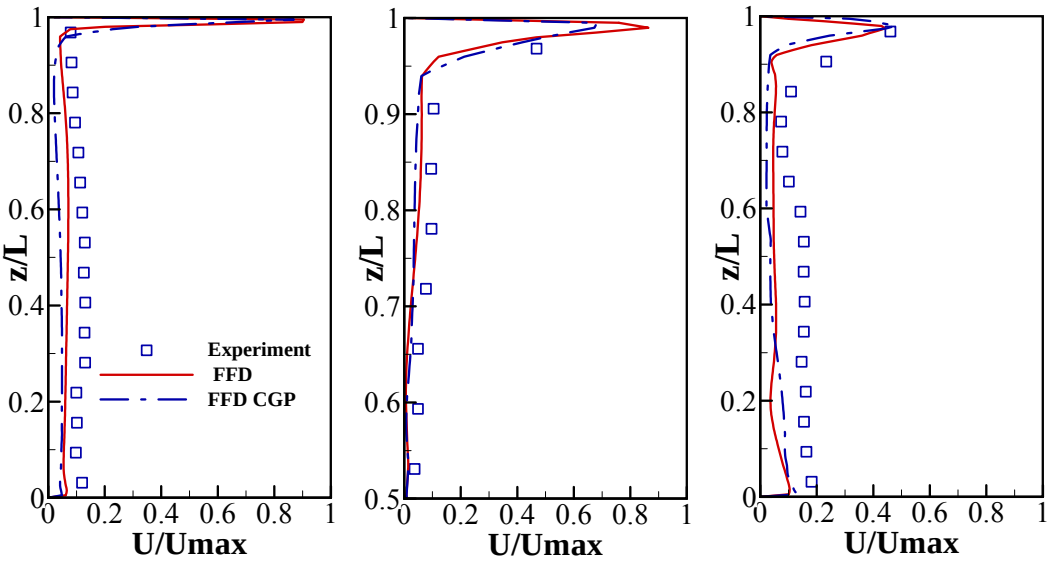

Figure 7. Velocity profiles in the room with a box under forced convection: comparison of predictions by the FFD models with the experimental data from Wang and Chen (2009) at Positions (a) 1, (b) 3, and (c) 5.

Because interaction between buoyancy convection and forced convection is a very common airflow feature in buildings, this study further applied FFD with the CGP scheme to simulate mixed ventilation in the chamber. The box was heated at a rate of 700 W, which generated thermal plumes that interacted with the jet flow from the air supply. Figure 8 compares the velocity profiles predicted by FFD with the experimental data. At Positions 1 and 2, similar vertical velocity profiles were predicted by FFD with and without the CGP scheme, and the profiles agreed very well with the experimental data. As in the case of forced ventilation in the empty room, both FFD models in the current case predicted velocity profiles with large discrepancies at Position 5 as compared with the experimental data, because of the complex flow structure near the right wall.

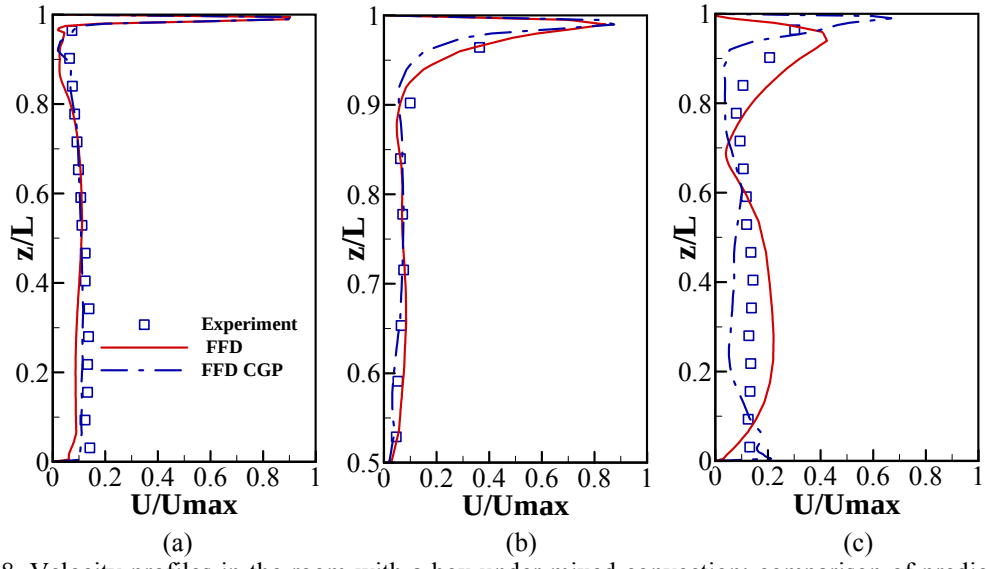

Figure 8. Velocity profiles in the room with a box under mixed convection: comparison of predictions by the FFD models with the experimental data from Wang and Chen (2009) at Positions (a) 1, (b) 3, and (c) 5.

When the performance of FFD with the CGP scheme was tested in the three cases above, it was found that the scheme would not have an observable influence on the accuracy of FFD in simulating building airflows. FFD accuracy was affected primarily by the lack of turbulence models or diffusive numerical algorithms.

Wind-Driven Cross Natural Ventilation. FFD is a potential tool for architects and engineers in designing natural ventilation in the early stages of building design. This study further investigated the impact of the CGP scheme on the performance of FFD in simulating natural ventilation. Wind is one of the main driving forces of natural ventilation, and therefore a wind-driven cross ventilation case based on the experiment conducted by Jiang et al. (2003) was used to test FFD with coarse-grid projection. The experiment measured the airflow through a scaled building model with two openings, in a wind tunnel. As depicted in Figure 9, the building had two openings of the same size on opposite walls. The dimensions used in the model were 250 mm × 250 mm × 250 mm for the building and 84 mm × 0.125 mm for the opening. A grid resolution of 52 × 36 × 50 was applied in the FFD simulation.

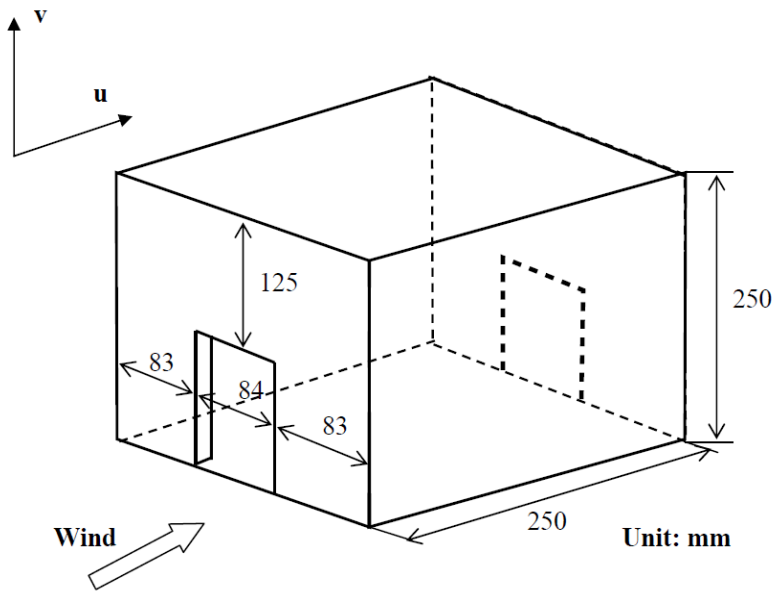

Figure 9. Schematic view of the building model for cross ventilation (Jiang et al., 2003).

A velocity profile following the logarithmic law was measured at the inlet of the wind tunnel, and the velocity profile was applied as an inlet boundary condition in the simulation. The vertical velocity distribution was measured along ten vertical lines in the streamwise direction and used as reference data for this study. The measurement locations are shown in Figure 10.

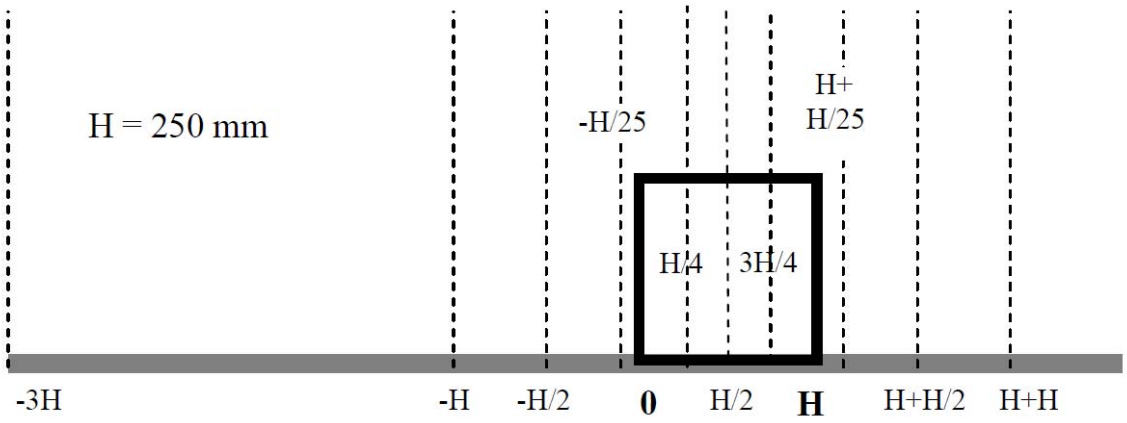

Figure 10. The positions at which velocity was measured in the streamwise mid-section of the wind tunnel (Jiang et al., 2003).

Figure 11 compares the velocity profiles along the streamwise locations as predicted by the two FFD models with the corresponding experimental data. FFD with and without the CGP scheme predicted very similar velocity profiles at the four measurement locations. On the upstream side of the building (X = -H/25), the velocity profiles predicted by both models agreed well with the experimental data. In regard to the velocity distribution in the building model (X = H/2), both models were able to predict the main velocity variation in the building, and FFD with the CGP scheme obtained better agreement with experimental data at this location. In the region near the leeward wall (X = H + H/25), the velocity profiles simulated by both FFD models agreed well with the experimental data. However, downstream from the building model (X = H + H/2), neither FFD model could achieve an accurate simulation of the wake region. Previous studies (Allocca, 2001) also found that it was difficult for CFD models to predict the velocity distribution accurately in the wake region behind the building model. Overall, FFD with the CGP scheme was able to predict the primary airflow distribution with reasonably good accuracy for wind-driven cross natural ventilation.

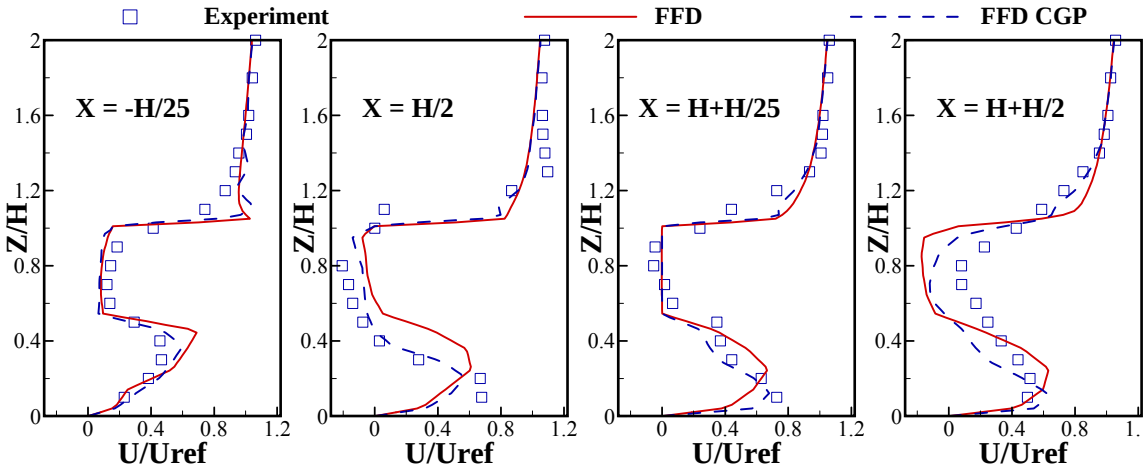

Figure 11. Velocity distributions in the streamwise direction: comparison of FFD predictions with experimental data.

Because the pressure projection was applied to enforce the conservation of mass in every cell in the computational domain, the airflow rate through the two openings of the building model should have been the same, whether the pressure equation was solved exactly or solved with a very small residual. In FFD, the maximum number of iterations was limited for the pressure equation solver, and thus it was possible that mass conservation was not fully satisfied during the simulation. This study examined the variation in predicted airflow rate through the openings during the simulation and further tracked the variation in mass

imbalance rate between the inlet and outlet of the building model. As shown in Figure 12, although both FFD models predicted the ventilation rate with reasonably good accuracy, FFD with the CGP scheme required considerably fewer time steps to reach a stabilized result. Meanwhile, the airflow rate predicted by the original FFD model exhibited intense fluctuation during the simulation, and many more time steps were required to obtain a stable result. An examination of the mass imbalance rate between two openings shows that the original FFD model also required more time steps than FFD with the CGP scheme to reduce the mass imbalance rate to a negligible value. Thus, the CGP scheme was able to improve the efficiency of FFD in achieving fully mass-conservative airflow simulations.

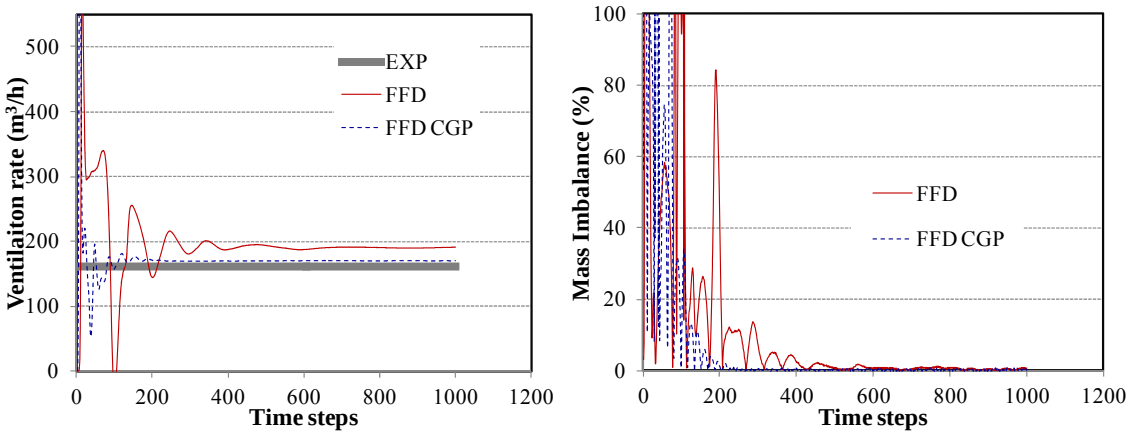

(a) (b)

Figure 12. Variations in (a) ventilation rate and (b) mass imbalance rate during the simulation as predicted by FFD with and without the CGP scheme.

Buoyancy-Driven Natural Ventilation. This study further tested the performance of FFD with the CGP scheme in simulating buoyancy-driven natural ventilation in a chamber with a door opening (Jiang and Chen, 2003). As shown in Figure 13(a), a test chamber in a laboratory was used to simulate the indoor environment, while the laboratory space simulated the outdoor environment. The airflow was driven by the buoyancy force generated by a 1500 W baseboard heater placed in the corner of the test chamber, and the stack pressure in the test chamber resulted in air change at the door opening. This study applied a grid resolution of 52 × 28 × 36 in the FFD simulation, and the wall surface temperature measured in the experiment was used as a boundary condition in the simulation. The velocity profiles simulated by FFD were compared to the experimental data measured at five positions, as shown in Figure 13(b).

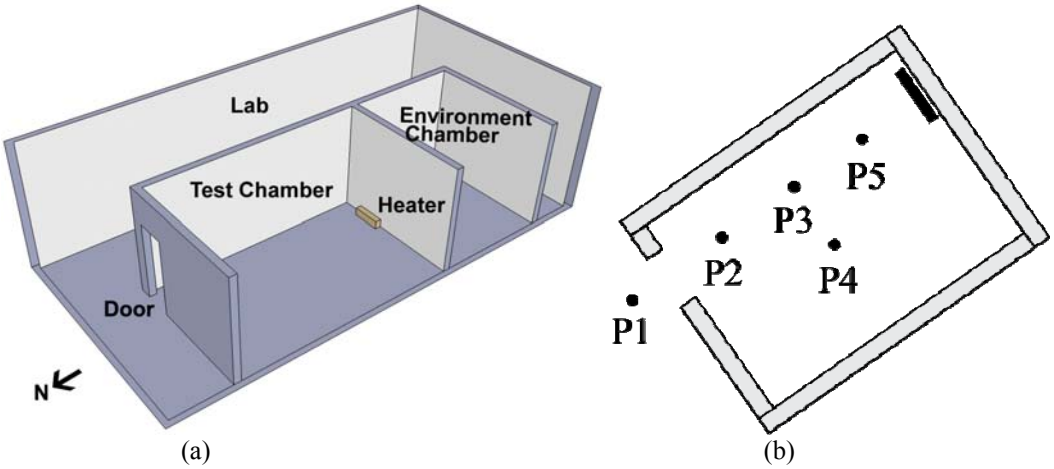

(a) (b)

Figure 13. Schematic of (a) the layout of the laboratory and (b) the measurement positions.

As shown in Figure 14, although the velocity profiles predicted by FFD with the CGP scheme showed some discrepancies with the measured velocity distribution at the four positions, the new FFD model was still able to capture the high velocity near the ceiling and the floor and the low velocity at the midpoint height inside the chamber. Meanwhile, the original FFD model exhibited the same simulation performance and was able to predict only the major airflow characteristics in the chamber with reasonable accuracy. Thus, the CGP scheme would not affect the performance of FFD in simulating buoyancy-driven natural ventilation.

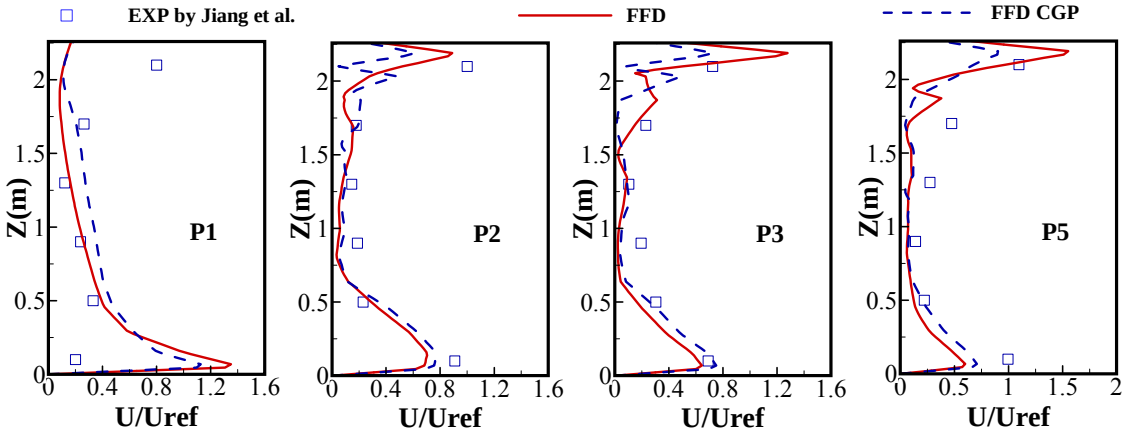

Figure 14. Comparison of the computed velocity profiles with the experimental data at the four measurement positions.

In a similar manner, this study examined the variation in air change rate at the door opening of the chamber during the simulation, as shown in Figure 15(a). The ventilation rate predicted by both FFD models agreed reasonably well with the experimental data. Although Figure 15(a) indicates that both FFD models required a similar number of time steps to obtain a steady ventilation rate, the ventilation rate predicted by the original FFD model showed much more intense fluctuation during the simulation. The mass imbalance rate in the simulation with the original FFD model exhibited a strong oscillation until it was gradually dampened to zero, as shown in Figure 15(b). However, FFD with the CGP scheme was much more efficient in reducing the mass imbalance rate. This result also proves that the CGP scheme enhanced the efficiency of FFD in achieving fully mass conservative airflow simulations.

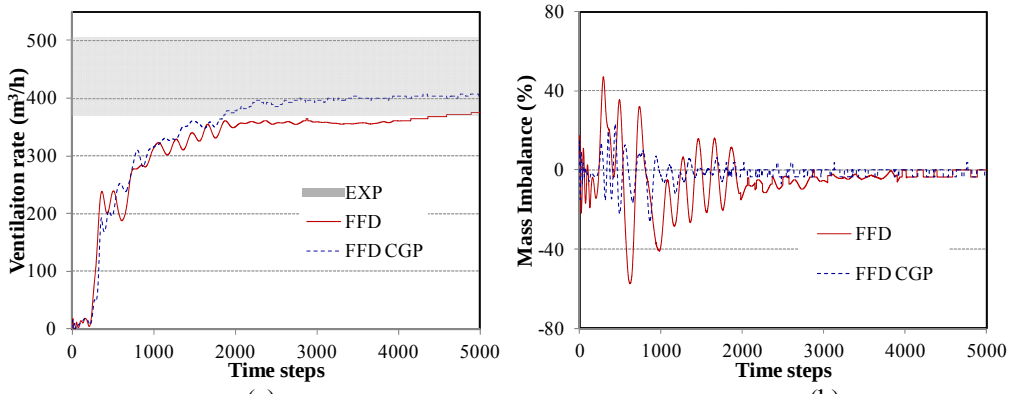

(a) (b)

Figure 15. Variations in (a) ventilation rate and (b) mass imbalance rate during the simulation as predicted by FFD with and without the CGP scheme.

Discussion

The tests above proved that the CGP scheme would have a negligible impact on the simulation accuracy of FFD and that it could efficiently reduce the computing effort of FFD in solving the pressure

equation. This study therefore compared the simulation speed of FFD with and without the CGP scheme with the speed of laminar CFD. In this study, the three models were applied to simulate test cases with the same grid number. All three cases used a time step size of 0.1 seconds, and the simulations were performed on a personal computer with a single Intel CPU at 3.00 GHz. The physical time and computing time for a simulation of 1000 time steps were recorded for the three models.

Table 1 presents the computing time required by the three models for each test case. Although the original FFD model was much more efficient than the CFD model, the FFD model with the CGP scheme required the least computing time for the simulation. Because the complexity of the airflows differed among the three cases, the computing speed may also have varied. However, according to the test cases in this study, the CGP scheme was able to accelerate FFD by approximately 1.5 times. FFD with the CGP scheme achieved a computing time that was 30 to 50 times faster than that of the CFD model. Therefore, in FFD simulations of airflows in and around buildings, the CGP scheme can significantly reduce simulation time without compromising accuracy.

Table 1 Comparison of computing time required by the FFD models and the CFD model.

Case	Grid	Physical time (s)	Computing time (s)		
			CFD	FFD	FFD CGP
Lid-driven cavity	32 × 32 × 32	100	4755	117	85
Forced ventilation	26 × 34 × 26	100	2287	87	56
Forced ventilation with box	28 × 36 × 28	100	3001	104	68
Mixed ventilation	28 × 36 × 28	100	3093	141	91
Cross ventilation	52 × 36 × 50	100	9730	329	227
Single-side ventilation	52 × 28 × 36	100	5345	234	160

Conclusions

This study investigated and implemented the CGP scheme in FFD in order to reduce the computing effort required to solve the pressure equation and thus accelerate FFD simulation of building airflows. A four-step approach was proposed for integration of the CGP scheme in FFD. After the momentum equations had been solved on the fine grid level, FFD first mapped the velocities on the fine grid level to the coarse grid level. The pressure equation was then solved on the coarse grid level, and the predicted pressure distribution was applied to correct the velocities on the coarse grid level. The same correction was prolongated to the fine grids and applied for the velocities at the fine cell faces that overlapped with coarse cell faces. A local projection was then applied to correct the inner velocities within each coarse cell, in order to achieve a divergence-free field on the fine grid.

This study applied FFD with the CGP scheme to simulate building airflows of varying complexity, including a typical room airflow pattern from a wall jet; forced and mixed ventilation in a chamber; wind-driven cross ventilation in a wind tunnel; and buoyancy-driven, single-sided ventilation in a full-scale chamber. The results showed that the CGP scheme did not have a negative impact on the accuracy of FFD in simulating building airflows, and it significantly reduced the fluctuations that occurred within the simulations. FFD with the CGP scheme required fewer time steps to obtain fully mass-conservative airflow simulations. In regard to computational efficiency, the CGP scheme was able to accelerate FFD by approximately 1.5 times, and FFD with the CGP scheme achieved a computing speed that was 30 to 50 times faster than that of the CFD model.

References

Allocca, C., 2001. Single-sided natural ventilation: design analysis and general guidelines. Massachusetts Institute of Technology.

Axley, J., 2007. Multizone airflow modeling in buildings: History and theory. *HVAC&R Research* 13(6), 907-928.

Behie, G., Forsyth, P., 1983. Multigrid solution of the pressure equation in reservoir simulation. *Society of Petroleum Engineers Journal* 23(04), 623-632.

Chorin, A.J., 1967. A numerical method for solving incompressible viscous flow problems. *Journal of Computational Physics* 2(1), 12-26.

Fedkiw, R., Stam, J., Jensen, H.W., 2001. Visual simulation of smoke, *Proceedings of the 28th annual conference on Computer graphics and interactive techniques. ACM,* 15-22.

Ferziger, J.H., Perić, M., 1999. Computational Methods for Fluid Dynamics. Springer, New York.

Fuchs, L., Zhao, H.S., 1984. Solution of three-dimensional viscous incompressible flows by a multi-grid method. *International Journal for Numerical Methods in Fluids* 4(6), 539-555.

Gray, Donald D., Aldo Giorgini, 1976. The validity of the Boussinesq approximation for liquids and gases. *International Journal of Heat and Mass Transfer* 19(5), 545-551.

Jiang, Y., Alexander, D., Jenkins, H., Arthur, R., Chen, Q., 2003. Natural ventilation in buildings: measurement in a wind tunnel and numerical simulation with large-eddy simulation. *Journal of Wind Engineering and Industrial Aerodynamics* 91(3), 331-353.

Jiang, Y., Chen, Q., 2003. Buoyancy-driven single-sided natural ventilation in buildings with large openings. *International Journal of Heat and Mass Transfer* 46(6), 973-988.

Jin, M., Zuo, W., Chen, Q., 2012a. Improvements of fast fluid dynamics for simulating air flow in buildings. *Numerical Heat Transfer, Part B: Fundamentals* 62(6), 419-438.

Jin, M., Zuo, W., Chen, Q., 2012b. Validation of three-dimensional fast fluid dynamics for indoor airflow simulations, *Proc. of 2nd Int. Conf. on Energy and Environment, Boulder, Colorado.*

Jin, M., Zuo, W., Chen, Q., 2013. Simulating natural ventilation in and around buildings by fast fluid dynamics. *Numerical Heat Transfer, Part A: Applications* 64(4), 273-289.

Ku, H.C., Hirsh, R.S., Taylor, T.D., 1987. A pseudospectral method for solution of the three-dimensional incompressible Navier-Stokes equations. *Journal of Computational Physics* 70(2), 439-462.

Lentine, M., Zheng, W., Fedkiw, R., 2010. A novel algorithm for incompressible flow using only a coarse grid projection. *ACM Transactions on Graphics (TOG)* 29(4), 114.

MacLachlan, S., Tang, J., Vuik, C., 2008. Fast and robust solvers for pressure-correction in bubbly flow problems. *Journal of Computational Physics* 227(23), 9742-9761.

McAdams, A., Sifakis, E., Teran, J., 2010. A parallel multigrid Poisson solver for fluids simulation on large grids, *Proceedings of the 2010 ACM SIGGRAPH/Eurographics Symposium on Computer Animation. Eurographics Association*, 65-74.

San, O., Staples, A.E., 2013a. A coarse-grid projection method for accelerating incompressible flow computations. *Journal of Computational Physics* 233(15), 480-508.

San, O., Staples, A.E., 2013b. An efficient coarse grid projection method for quasigeostrophic models of large-scale ocean circulation. *International Journal for Multiscale Computational Engineering* 11(5), 463-495.

Sidilkover, D., Ascher, U., 1995. A multigrid solver for the steady state navier-stokes equations using the pressure-poisson formulation. *Computation and Applied Mathematics* 14(1), 21-35.

Stam, J., 1999. Stable fluids, *Proceedings of the 26th annual conference on Computer graphics and interactive techniques.* ACM Press/Addison-Wesley Publishing Co., 121-128.

Staniforth, A., Côté, J., 1991. Semi-Lagrangian integration schemes for atmospheric models-a review. *Monthly Weather Review* 119(9), 2206-2223.

Tatebe, O., 1993. The multigrid preconditioned conjugate gradient method, *NASA Conference Publication. NASA*, pp. 621-621.

Wang, M., Chen, Q., 2009. Assessment of Various Turbulence Models for Transitional Flows in an Enclosed Environment (RP-1271). *HVAC&R Research* 15(6), 1099-1119.

Zuo, W., Chen, Q., 2009. Real-time or faster-than-real-time simulation of airflow in buildings. *Indoor Air* 19(1), 33-44.

Zuo, W., Chen, Q., 2010a. Fast and informative flow simulations in a building by using fast fluid dynamics model on graphics processing unit. *Building and Environment* 45(3), 747-757.

Zuo, W., Chen, Q., 2010b. Simulations of air distributions in buildings by FFD on GPU. *HVAC&R Research* 16(6), 785-798.
Zuo, W., Hu, J., Chen, Q., 2010. Improvements in FFD modeling by using different numerical schemes. *Numerical Heat Transfer, Part B: Fundamentals* 58(1), 1-16.
Zuo, W., Jin, M., Chen, Q., 2012. Reducaiton of numrical diffusion in FFD model. *Engineering Applications of Computational Fluid Mechanics* 6(2), 234-247.